RSC Advances

ROYAL SOCIETY OF CHEMISTRY

www.rsc.org/advances

Dissipative particle dynamics study of nano-encapsulated thermal energy storage phase change material

Zhonghao Rao*, Xinyu You, Yutao Huo, Xinjian Liu

School of Electric Power Engineering, China University of Mining and Technology, Xuzhou 221116 China

Abstract

The nano-encapsulated phase change materials (PCM), which have many good thermophysical properties, were proposed as potential for thermal energy storage. Considered various PCM have been widely researched on micro and macro perspective by experimental and simulated method, to form a bridge between microstructure and macroscale properties of nano-encapsulated PCM, in this study, the dissipative particle dynamics (DPD) simulation method was used to investigate the mesoscopic morphologies and evolution mechanisms of the nano-encapsulated PCM. The coarse-grained and Flory-Huggins-type models were used to obtain the molecular structures and interaction parameters. The results showed that the nano-encapsulated PCM can be fabricated by using n-docosane as core material and styrene (St), ethyl acrylate (EA) and allyloxy nonylphenoxy propanol polyoxyethylene ether ammonium sulfate (DNS-86) as shell materials. The core-shell structures fail to fabricate with excess surfactant and shell materials. The preliminary optimized encapsulation rate of core material could be useful for the design and experiment of nano-encapsulated PCM.

Keywords: Nano-encapsulated phase change material, Thermal energy storage, Dissipative particle dynamics, Coarse-grained, Interaction parameter

* Corresponding author. Tel.: +86 516 83592000. E-mail address: raozhonghao@cumt.edu.cn.

1. Introduction

Energy shortage and environmental pollution have attracted worldwide attention in the past decades; simultaneously many researchers throughout the world have devoted their lives to searching renewable and energy-saving technologies for sustainable development of economy and society. To avoid large reduction in energy system, thermal energy storage, a vital role in renewable energy and waste heat recovery, is of growing importance. [1] With many good thermophysical properties such as suitable phase-transition temperature, high latent heat of transition and good heat transfer, phase change materials (PCM) have been proposed as a viable solution for thermal energy storage. [2, 3] Morever, the PCM have been widely used in various fields for thermal management or transportation including greenhouses, [4] buildings, [5, 6] solar energy, [7] electronic devices, [8] electric vehicle batteries, [9] and many others.

To overcome the inherent disadvantages such as corrosive to metal, decomposition, sub-cooling and leakage of different PCM, encapsulation of PCM is an effective solution. [10] PCM capsules in micro and nano-scale (i.e. micro/nano-encapsulated PCM) have been utilized in many fields especially in latent functionally thermal fluids or slurries. [11, 12] Compared with micro-encapsulated PCM, the nano-encapsulated PCM showed better performance such as well repeated cycling and lower viscosity that can be used in fluid and textile field. [10, 13] The PCM capsules have been developed widely, most of the works focus on micro-encapsulated PCM. There is limited literature for studying nano-encapsulated PCM. Zhang et al. [14] fabricated nano-capsules containing n-octadecane with melamine-formaldehyde shell

and analyzed the effects of stirring rate on the diameters and morphology of capsules, and latter, Fang et al. [10] indicated that a stirring rate 1500rpm was suitable for the nano-encapsulation. Park et al. [15] synthesized polystyrene particles by encapsulated paraffin wax as PCM. Su et al. [16] described the heat transfer property of a single-phase liquid by adding nano-encapsulated PCM. All the above works are carried out at the micro perspective (structure and morphology) and macro perspective (preparation and properties). In our previous work, we have investigated the themal behavior of PCM by molecular dynamics (MD) simulations method from the microscopic scale. [17, 18, 19] However, research addressing nano-encapsulated PCM has rarely been performed in the mesoscopic perspective. Dissipative particle dynamics (DPD), introduced by Hoogerbrugge and Koelman, [20] has been applied to study the mesostructures and morphology evolution of many materials. The DPD method, with coarse-graining procedure, forms a bridge between fast molecular kinetics and the slow thermodynamic relaxation of macroscale properties. [21]

In the present work, the DPD method is employed to interpret the mesostructures and morphology evolution of the nano-encapsulated PCM. Compared with our previous study, [22, 23] the contents of core and shell mateirals in the PCM system are more complex. This attempt studies also discussed the effect of shell and core materials content on morphology of the PCM.

2. Method and model

3.1 DPD theory

In the DPD model, a group of molecules or a volume of fluid was represented as a DPD bead, and many of these interacting beads form a mesoscopic system. [24, 25] The time evolution of motion for the DPD beads can be obtained by Newton's equations of motion: [26, 27]

$$\frac{dr_i}{dt} = v_i, m_i \frac{dv_i}{dt} = f_i \quad (1)$$

where f_i, m_i, r_i, and v_i are the force, mass, position vectors, and velocity vectors of bead i, respectively. The mass of each bead is usually set to 1 DPD mass unit. [26] The force between each pair of beads is composed of four types: [28, 29]

$$f_i = \sum_{j \neq i}(F_{ij}^C + F_{ij}^D + F_{ij}^R + F_i^S) \quad (2)$$

where F_{ij}^C, F_{ij}^D, and F_{ij}^R are the conservative force, dissipative force, and random force of bead i and j, respectively. F_i^S is the spring force. Different parts of the forces are given by

$$F_{ij}^C = \begin{cases} -a_{ij}(1 - r_{ij}/r_c)\hat{\boldsymbol{r}}_{ij}, & r_{ij} < r_c \\ 0, & r_{ij} > r_c \end{cases} \quad (3)$$

$$F_{ij}^D = \frac{\sigma^2[\omega(r_{ij})]^2}{2kT}(\boldsymbol{v}_{ij} \cdot \hat{\boldsymbol{r}}_{ij})\hat{\boldsymbol{r}}_{ij} \quad (4)$$

$$F_{ij}^R = \begin{cases} \frac{\sigma\omega(r_{ij})\hat{\mathbf{r}}_{ij}\xi_{ij}}{\sqrt{\delta_t}}, & r_{ij} < r_c \\ 0, & r_{ij} > r_c \end{cases} \quad (5)$$

$$F_i^S = \sum_j C\,\boldsymbol{r}_{ij} \quad (6)$$

where a_{ij} is the maximum repulsion between beads i and j.[30] $\boldsymbol{r}_{ij} = \boldsymbol{r}_i - \boldsymbol{r}_j$, $r_{ij} = |\boldsymbol{r}_{ij}|$, $\hat{\mathbf{r}}_{ij} = \boldsymbol{r}_{ij}/r_{ij}$, $\boldsymbol{v}_{ij} = \boldsymbol{v}_i - \boldsymbol{v}_j$. r_c is the cutoff radius, which always set to be 1 unit of length in simulations. $\omega(r)$ stands for r-dependent weight function $\omega(r) = (1 - r)$ for r <1 and $\omega(r) = 0$ for r > 1. ξ_{ij} is a random number with zero mean and unit variance. σ is the noise strength and was set as 3, and δ_t is the time step of simulation. C is the spring constant and in this study the default value of C is

4.

In the beginning, Euler-type algorithm was used to integrate the set of positions and velocities. [20, 28] And then they developed a modified version of the velocity-Verlet algorithm: [26, 31]

$$\boldsymbol{r}_i(t+\Delta t) = \boldsymbol{r}_i(t) + \Delta t \boldsymbol{v}_i(t) + \frac{1}{2}(\Delta t)^2 \boldsymbol{f}_i(t) \quad (7)$$

$$\widetilde{\boldsymbol{v}}_i(t+\Delta t) = \boldsymbol{v}_i(t) + \lambda \Delta t \boldsymbol{f}_i(t) \quad (8)$$

$$\boldsymbol{f}_i(t+\Delta t) = \boldsymbol{f}_i(\boldsymbol{r}(t+\Delta t), \widetilde{\boldsymbol{v}}_i(t+\Delta t)) \quad (9)$$

$$\boldsymbol{v}_i(t+\Delta t) = \boldsymbol{v}_i(t) + \frac{1}{2}\Delta t(\boldsymbol{f}_i(t) + \boldsymbol{f}_i(t+\Delta t)) \quad (10)$$

As the mass of each bead is usually set to 1, the force acting on a bead equals its acceleration $\widetilde{\boldsymbol{v}}_i(t+\Delta t)$. The force is still updated once per iteration without increase in computational cost. Hence, the modified velocity-Verlet algorithm is used in the current work.

3.2 Models and interaction parameters

To form nano-encapsulated PCM, the components used in this study contain water, n-docosane, Azodiisobutyronitrile (AIBN), polyvinyl pyrrolidone (PVP), octylphenol polyoxyethylene ether (OP-10), styrene (St), ethyl acrylate (EA) and allyloxy nonylphenoxy propanol polyoxyethylene ether ammonium sulfate (DNS-86). The coarse-grained models in this simulation are shown in Fig. 1. Each molecule of water, AIBN, St and EA are represented as bead a, c, g and h, respectively. An n-docosane molecule is divided into two beads b. Each monomer of PVP is considered as one bead d. A molecule of OP-10 is divided into two beads e and f, and

DNS-86, i and j.

Before calculating the conservation force, the repulsion parameters a_{ij} should be calculated. The link between the repulsive parameter a_{ij} and χ-parameters in Flory-Huggins-type models has been made by Groot and Warren. [26, 32] For the beads of a same type, the repulsion parameters a_{ii} is shown as: [31]

$$a_{ii}\rho = 75k_BT \quad (11)$$

where ρ=3 and k_BT=1 were usually used in many previous works. [33, 34, 35, 36] ρ is the density, T is the system temperature and k_B is the Boltzmann constant. The repulsion parameters between different types of beads, a_{ii} are shown as:[27]

$$a_{ij} = a_{ii} + 3.27\chi_{ij} \quad (12)$$

where the value of a_{ij} can be obtained from solubility parameters:

$$\chi_{ij} = \frac{V_{bead}}{kT}(\delta_i - \delta_j)^2 \quad (13)$$

where V_{bead} is the average molar volume of two beads. δ_i and δ_j are the solubility parameters of bead i and j.

The solubility parameters used in the current research are calculated by MD simulations. The details of the MD processes can be seen in our previous study. [18, 23, 37] Each MD system consists of more than 1 000 atoms in a cubic cell of amorphous structure with periodic boundary conditions. The smart minimization method was used to optimize the geometry. Then 100 ps in constant-temperature, constant-pressure ensemble (NPT), and 100 ps in constant temperature, constant volume ensemble (NVT) was used to equilibrate the system. After equilibration, 1 000 ps were used in NPT ensemble to analyze the molar volume and solubility parameter.

All the simulations were performed using Amorphous Cell, Discover and Forcite modules in Materials Studio 5.5 software (Accelrys) with the condensed-phase optimized molecular potentials for atomistic simulation studies (COMPASS) force field. [38, 39] The simulated molar volumes and solubility parameters of beads is shown in Table 1. According to Eqs.(11)-(13), the calculated interaction parameters of different beads at 298 K used in the following DPD simulation are given in Table 2.

A cubic box with a size of 32 × 32 × 32 with periodic boundary conditions (PBC) was adopted in this work after checked the influence of box sizes on the simulation results. The total number of beads is 9.8×10^4. The time step was taken as 0.05 and 40 000 steps were adopted to obtain equilibration phase. All the simulations were carried out using DPD program incorporated in the Materials Studio 5.5 software (Accelrys) with a constant temperature.

3. Results and discussion

A possible proportion, which according to published work such as Fang et al., [10] of the components (n-docosane: St: EA: DNS-86: PVP: OP-10: AIBN) used in the DPD simulation is 10:8:0.25:0.6:0.08:0.8:0.04 and the water is sufficient for the dynamic process. Fig.2 shows the evolution of the diffusivity of different beads with the simulation time. In a typical simulation, the diffusivity decreases rapidly at the first 400 DPD units (8 000 time steps). After about 1 600 DPD units, it can be seen that the diffusivity gradually tend to a steady state. This indicates that a time of 2 000 DPD units are long enough to meet the system achieving equilibrium.

In the nano-encapsulated PCM system, n-docosane was used as core material and St, EA and DNS-86 were used as shell materials and other components were used as surfactant. Fig. 3 clearly shows the change of aggregates with increasing simulation steps in the simulated nano-encapsulated PCM system with a possible proportion as 10:8:0.25:0.6:0.08:0.8:0.04. The beads which represent water and other components have been removed from the figures so that morphologies of the capsule structure could be clearly seen. At first (t=0 step), different beads which represent the shell and core materials are distributed randomly in the cubic box. At t=1 000 steps, different structure transition can be observed. And some n-docosane molecules started aggregate together at the time of t=5 000 steps. Finally, ordered spherical capsule structure is formed at t=30 000 steps and the spherical capsule structure did not change significantly until t=40 000 steps. From the capsule, we can found that the n-docosane molecules are encapsulated with St, EA and DNS-86. The core-shell structure indicated that the nano-encapsulated PCM were fabricated the phenomenon also confirmed the feasibility of DPD method in understanding the aggregates dynamic process of nano-encapsulated PCM system.

In the preparation of the nano-encapsulated PCM, the content of surfactant is far less than the content of shell and core materials. However, the surfactants in the experiment are very important with the roles such as initiator, emulsifier and dispersant. Therefore, in the DPD simulations, the interactions of different surfactants are also considered although the chemical reaction is ignored in the dynamic process. For preliminary understanding the effect of the concentration of surfactant on the

capsule structure in the nano-encapsulated PCM system, Fig.4 shows the Iso-density surfaces of AIBN with different AIBN content: (a) 0.04, (b) 6; and PVP with different PVP content: (c) 0.08, (d) 2; and OP-10 with different OP-10 content: (e) 0.8, (f) 9, at t=40 000 DPD steps. As can be seen in Fig.4(a),(b), the AIBN distributed intricately and showed embedded trends when the proportion of AIBN is possible real proportion. When the proportion of AIBN is excess the possible proportion too much such as ten times, the Iso-density surfaces of AIBN are observed as cylindrical structure that the n-docosane can not be encapsulated. As can be seen in Fig.4(c),(d), the Iso-density surfaces of PVP display cluster structure when the proportion of PVP is excess and it is unnecessary and adverse for fabricating nano-encapsulated PCM. Analogously, as can be seen in Fig.4(e),(f), when the proportion of OP-10 is proper, the OP-10 is distributed uniformly on the surface of the PCM capsule. And the nano-encapsulated PCM also can not be fabricated when the proportion of OP-10 is excess.

The shell of the nano-encapsulated PCM contains a small amount of EA and DNS-86; we varied also the Iso-density surfaces of the shells by varying the preparation of EA and DNS-86. Fig.5 shows the Iso-density surfaces of EA at 4×10^4 DPD steps with different EA content: (a) 0.25, (b) 4; and DNS-86 at 4×10^4 DPD steps with different DNS-86 content: (c) 0.6, (d) 3. As can be seen in Fig.5(a),(c), both EA and DNS-86 are presented with typical spherical shell structure when the proportions of EA and DNS-86 are proper. Likewise, the cylindrical structure can be observed when the contents of EA and DNS-86 are too large. This also indicated that the nano-encapsulated PCM can not be fabricated.

The shell of the nano-encapsulated PCM contains St, EA and DNS-86 that it is complex to predict a more possible encapsulation rate of n-docosane by adjusting the proportion of shell materials. Hence, the content of bead ‘b’ which represents the core material was adjusted in the DPD simulation. Fig.6 shows the evolution of the diffusivity of bead ‘b’ with different n-docosane content. It can be seen that the diffusivity of bead ‘b’ with a content lower than 13 is close to zero at the last 400 DPD units. When the content is higher than 13, such as 14 and 15, the system achieved equilibrium but the diffusivity is still fluctuating at about 0.7 DPD units. It also can be concluded that the capsule structure of PCM did not fabricated. The encapsulation rate, which can be seen as the rate of core material and the whole PCM capsule, of n-docosane can be obtained as 54.51% and it can be used as reference for the preparation experiment. As the DPD method is based on the coarse-grained model, more accurate encapsulation rate of core material is worth to study further based on the development of force field.

4. Conclusions

In this work we investigated the mesoscopic morphologies and evolution mechanism of the nano-encapsulated PCM by DPD simulation method. By using n-docosane as core material and St, EA and DNS-86 as shell materials, the molecular structures employed in the encapsulation process were coarse-grained with a systematic coarse-graining strategy. When the proportion of the components is proper, a typical core-shell structure of the nano-encapsulated PCM can be obtained. The

PCM capsules fail to fabricate with excess surfactant and shell materials. A preliminary optimized encapsulation rate of n-docosane is 54.51% according to the DPD simulations. The DPD model described in this work could be useful in the design and experiment of nano-encapsulated PCM.

Acknowledgements

This work was supported by the natural science foundation of Jiangsu Province (BK20140190) and the Fundamental Research Funds for the Central Universities (China University of Mining and Technology, No. 2014QNA24).

References

[1] F. Pitie, C. Y. Zhao and G. Caceres, Energy Environ. Sci. , 2011, 4, 2117-2124.

[2] A. Sharma, V. V. Tyagi, C. R. Chen and D. Buddhi, Renew. Sust. Energ. Rev., 2009, 13, 318-345.

[3] E. Oró, A. de Gracia, A. Castell, M. M. Farid and L. F. Cabeza, Appl. Energy 2012, 99, 513-533.

[4] H. Benli and A. Durmuş, Sol. Energy 2009, 83, 2109-2119.

[5] A. M. Khudhair and M. M. Farid, Energy Convers. Manage. , 2004, 45, 263-275.

[6] D. Zhou, C. Y. Zhao and Y. Tian, Appl. Energy 2012, 92, 593-605.

[7] P. C. Eames and P. W. Griffiths, Energy Convers. Manage. , 2006, 47, 3611-3618.

[8] R. Kandasamy, X. Q. Wang and A. S. Mujumdar, Appl. Therm. Eng. , 2008, 28, 1047-1057.

[9] Z. H. Rao, S. F. Wang and G. Q. Zhang, Energy Convers. Manage. , 2011, 52, 3408-3414.

[10] Y. T. Fang, S. Y. Kuang, X. N. Gao and Z. G. Mang, Energy Convers. Manage. , 2008, 49, 3704-3707.

[11] J. L. Alvarado, C. Marsh, C. Sohn, G. Phetteplace and T. Newell, Int. J. Heat Mass Transfer 2007, 50, 1938-1952.

[12] X. Wang, R. L. Zeng, B. J. Chen, Y. P. Zhang, J. L. Niu, X. C. Wang and H. F. Di, Appl. Energy 2009, 86, 2661-2670.

[13] G. Cho and K. Choi, J. Appl. Polym. Sci. , 2011, 121, 3238-3245.

[14] X. X. Zhang, Y. F. Fan, X. M. Tao and K. L. Yick, Mater. Chem. Phys. , 2004, 88, 300-307.

[15] S. J. Park, K. S. Kim and S. K. Hong, Polym-Korea, 2005, 29, 8-13.

[16] M. Su, Y. Hong, S. J. Ding, W. Wu, J. J. Hu, A. A. Voevodin, L. Gschwender, E. Snyder and L. Chow, ACS Appl. Mater. Interfaces 2010, 2, 1685-1691.

[17] Z. H. Rao, S. F. Wang, M. C. Wu, Y. L. Zhang and F. H. Li, Energy Convers. Manage. , 2012, 64, 152-156.

[18] Z. H. Rao, S. F. Wang and F. F. Peng, Int. J. Heat Mass Transfer 2013, 64, 581-589.

[19] Z. Rao, S. Wang and F. Peng, Appl. Energy 2012, 100, 303-308.

[20] Hoogerbrugge P. J. and Koelman J. M. V. A., Europhys. Lett. , 1992, 19, 155-160.

[21] S. L. Yuan, X. Q. Zhang and K. Y. Chan, Langmuir, 2009, 25, 2034-2045.

[22] Z. H. Rao, S. F. Wang, F. F. Peng, W. Zhang and Y. L. Zhang, Energy, 2012, 44, 805-812.

[23] Z. Rao, Y. Huo and X. Liu, RSC Advances, 2014, 4, 20797.

[24] Y. Qian, X. D. Guo, L. J. Zhang and J. Zhou, Chem. Eng. J. , 2007, 131, 195-201.

[25] Z. Y. Lu, H. Wang, Y. T. Liu and H. J. Qian, Polymer, 2011, 52, 2094-2101.

[26] R. D. Groot and P. B. Warren, J. Chem. Phys. , 1997, 107, 4423-4435.

[27] Y. Qian, X. D. Guo, J. P. K. Tan, S. H. Kim, L. J. Zhang, Y. Zhang, J. L. Hedrick and Y. Y. Yang, Biomaterials, 2009, 30, 6556-6563.

[28] P. Espanol and P. Warren, Europhys. Lett. , 1995, 30, 191-196.

[29] G. H. Hu, J. G. Gai, H. L. Li, S. P. Zhu and S. Hoppe, Ind Eng Chem Res, 2010, 49, 11369-11379.

[30] D. Duong-Hong, N. Phan-Thien, K. S. Yeo and G. Ausias, Comput. Meth. Appl. Mech. Eng. , 2010, 199, 1593-1602.

[31] R. D. Groot and T. J. Madden, J. Chem. Phys. , 1998, 108, 8713-8724.

[32] H. Wen, H. Wu, J. B. Xu, X. F. He and Y. H. Zhao, Colloid Surface A, 2006, 290, 239-246.

[33] Z. T. Cai, S. L. Yuan, G. Y. Xu and Y. S. Jiang, Chem. Phys. Lett. , 2002, 365, 347-353.

[34] X. R. Cao, G. Y. Xu, Y. M. Li and Z. Q. Zhang, J. Phys. Chem. A 2005, 109, 10418-10423.

[35] H. L. Li, J. G. Gai, C. Schrauwen and G. H. Hu, Polymer, 2009, 50, 336-346.

[36] J. W. Jiang and Z. L. Luo, Polymer, 2010, 51, 291-299.

[37] Z. Rao, S. Wang and F. Peng, Int. J. Heat Mass Transfer 2013, 66, 575-584.

[38] H. Sun, J. Phys. Chem. B 1998, 102, 7338-7364.

[39] H. Sun, P. Ren and J. R. Fried, Comput. Theor. Polym. Sci. , 1998, 8, 229-246.

Figure captions:

Fig.1 Coarse-grained models of water (a), n-docosane (b), AIBN (c), PVP (d), OP-10 (e, f), St (g), EA (h) and DNS-86 (i, j)

Fig.2 Evolution of the diffusivity of different beads with the simulation time

Fig.3 Change of aggregates with increasing simulation steps in the simulated PCM system with PBC and a possible proportion as 10:8:0.25:0.6:0.08:0.8:0.04

Fig.4 Iso-density surfaces of AIBN with different AIBN content under PBC: (a) 0.04, (b) 6; and PVP with different PVP content: (c) 0.08, (d) 2; and OP-10 with different OP-10 content: (e) 0.8, (f) 9, at 4×10^4 DPD steps

Fig.5 Iso-density surfaces of EA at 4×10^4 DPD steps with different EA content under PBC: (a) 0.25, (b) 4; and DNS-86 at 4×104 DPD steps with different DNS-86 content: (c) 0.6, (d) 3

Fig.6 Evolution of the diffusivity of bead ‘b’ with different n-docosane content

Table captions:

Table 1 The molar volumes and solubility parameters of beads

Table 2 The interaction parameters of beads in PCM system

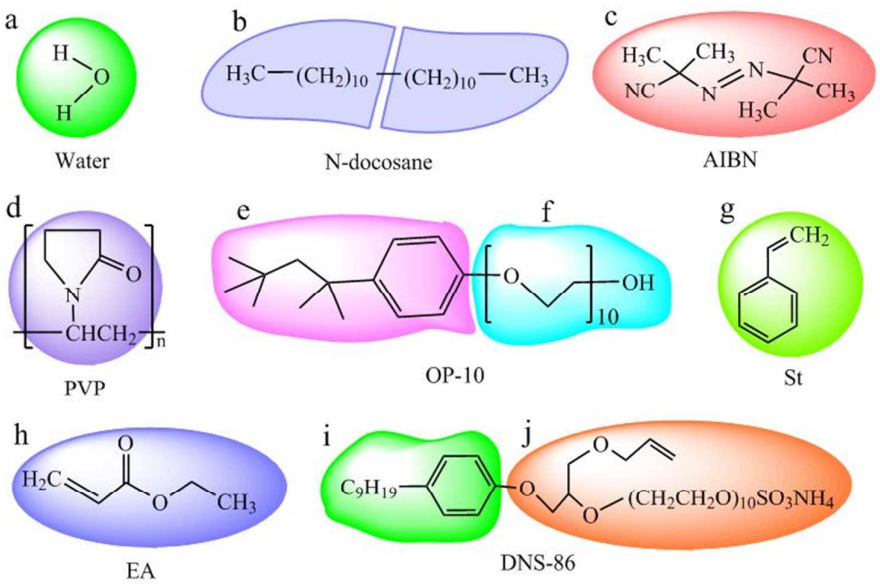

Fig.1 Coarse-grained models of water (a), n-docosane (b), AIBN (c), PVP (d), OP-10 (e, f), St (g), EA (h) and DNS-86 (i, j)

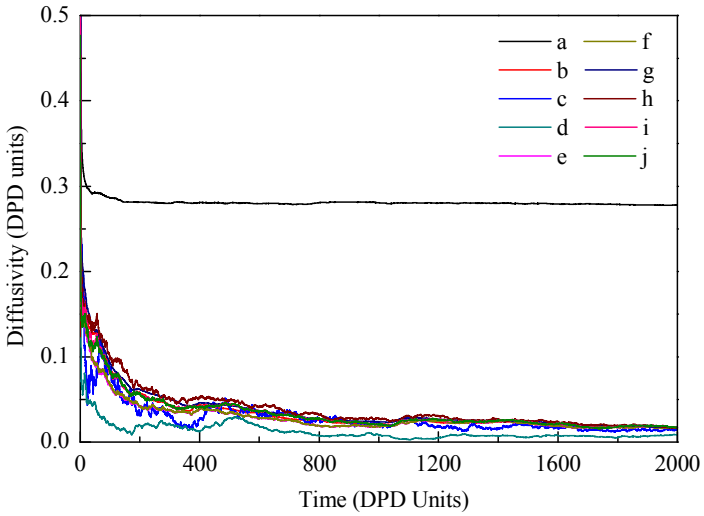

Fig.2 Evolution of the diffusivity of different beads with the simulation time

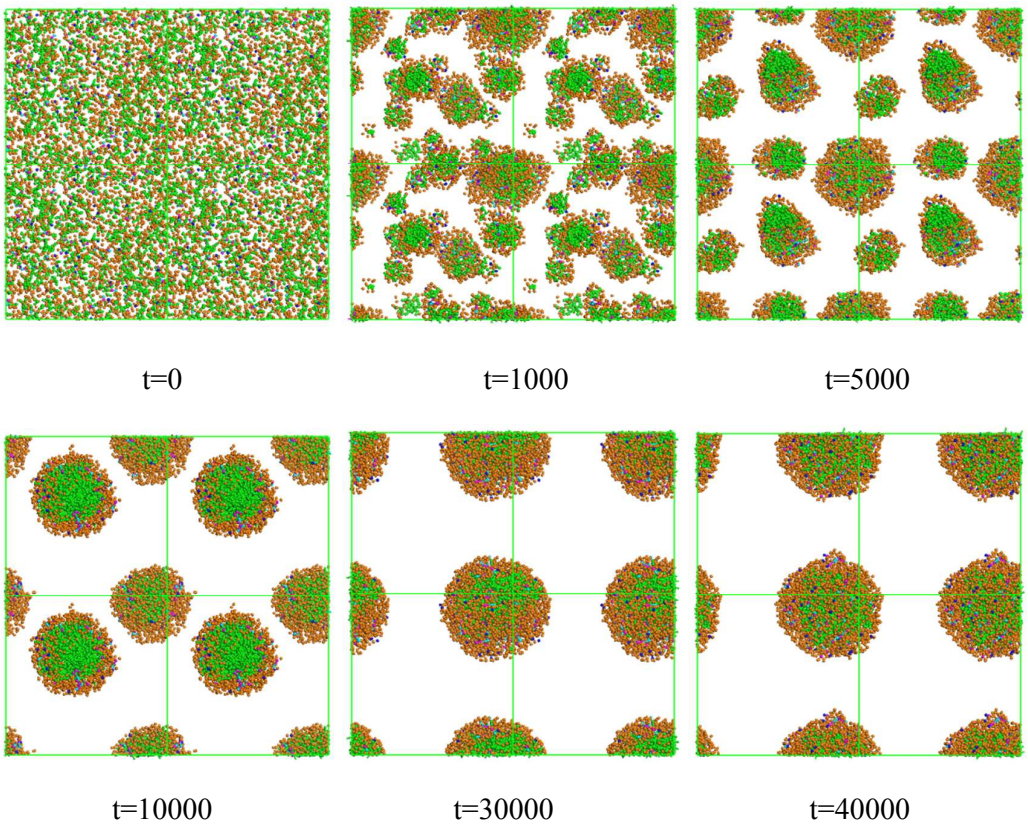

Fig.3 Change of aggregates with increasing simulation steps in the simulated PCM system with a possible proportion as 10:8:0.25:0.6:0.08:0.8:0.04

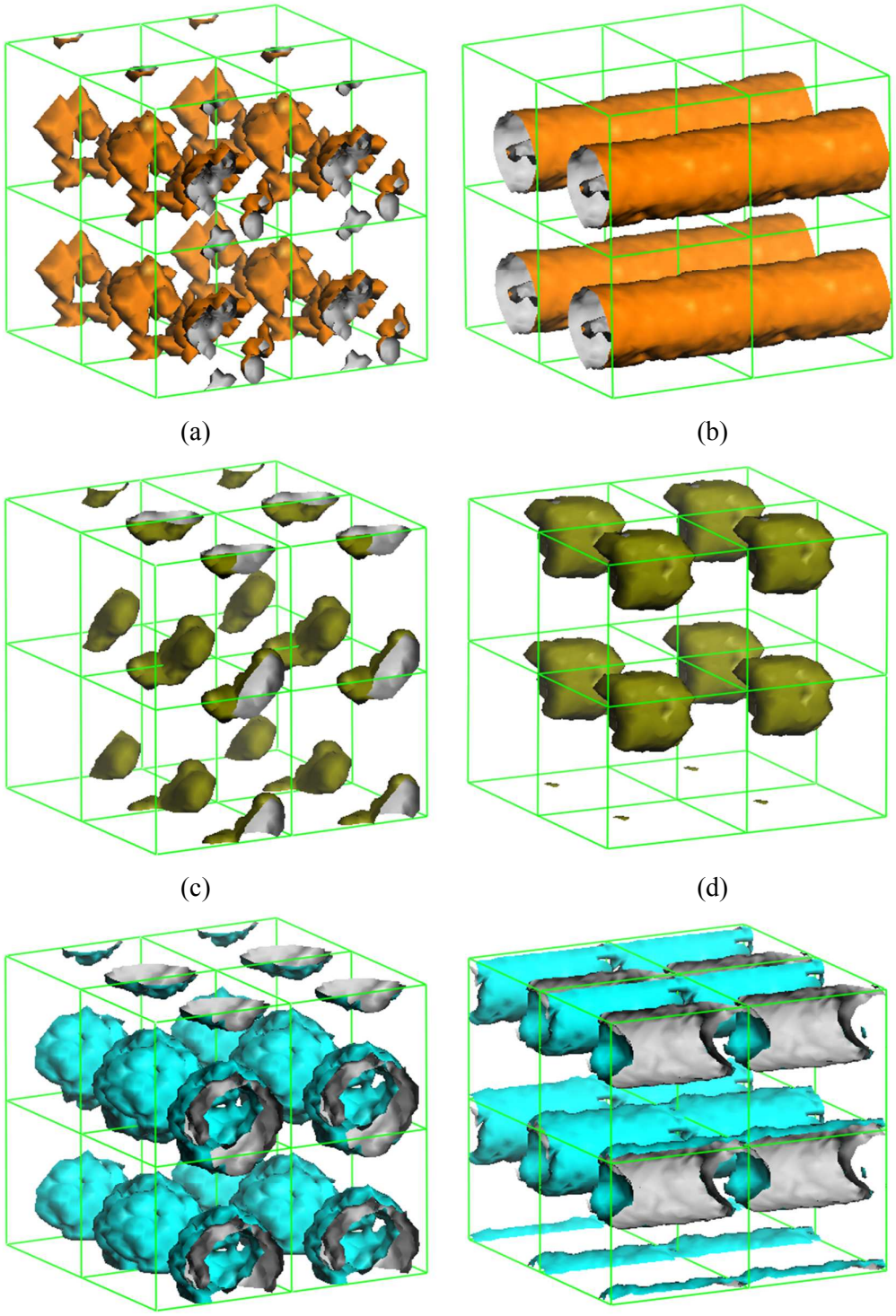

Fig.4 Iso-density surfaces of AIBN with different AIBN content: (a) 0.04, (b) 6; and PVP with different PVP content: (c) 0.08, (d) 2; and OP-10 with different OP-10 content: (e) 0.8, (f) 9, at 4×10^4 DPD steps

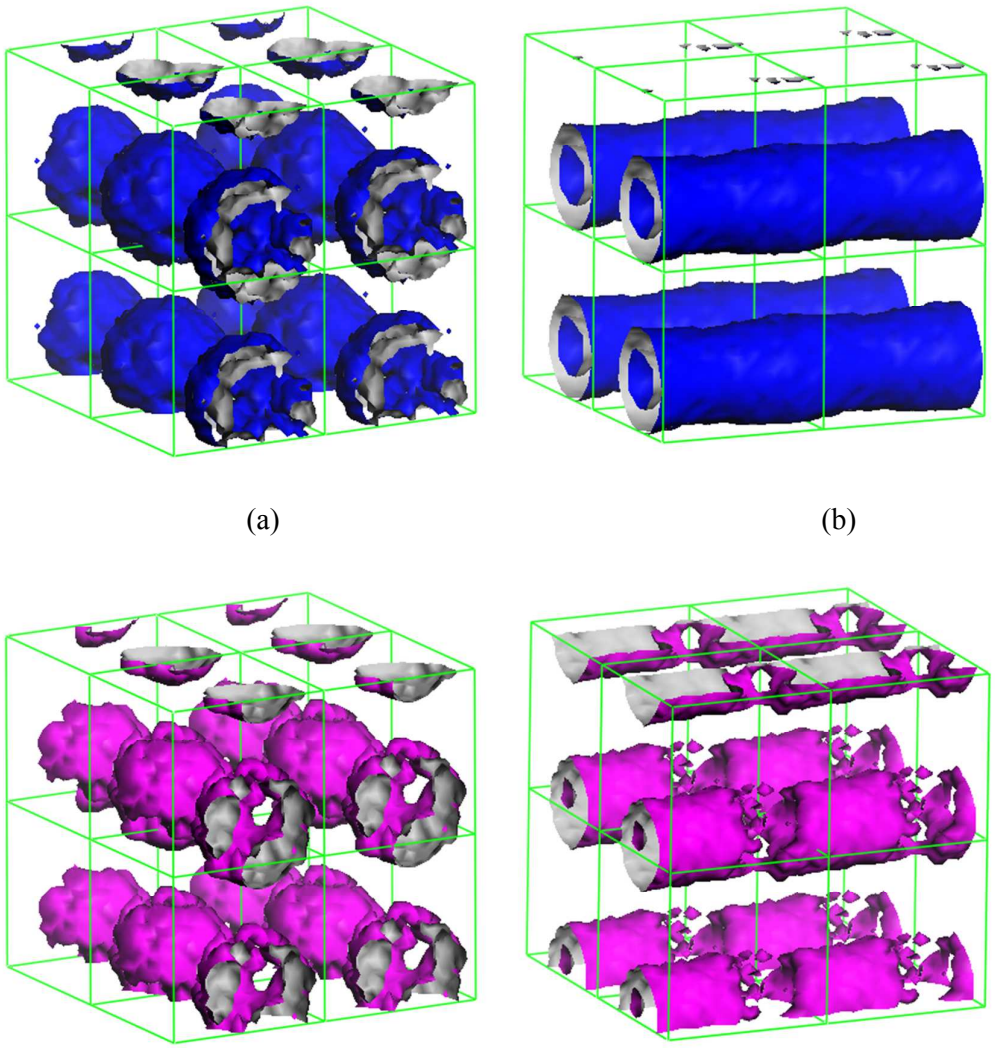

(a) (b)

(c) (d)

Fig.5 Iso-density surfaces of EA at 4×10^4 DPD steps with different EA content: (a) 0.25, (b) 4; and DNS-86 at 4×10^4 DPD steps with different DNS-86 content: (c) 0.6, (d) 3

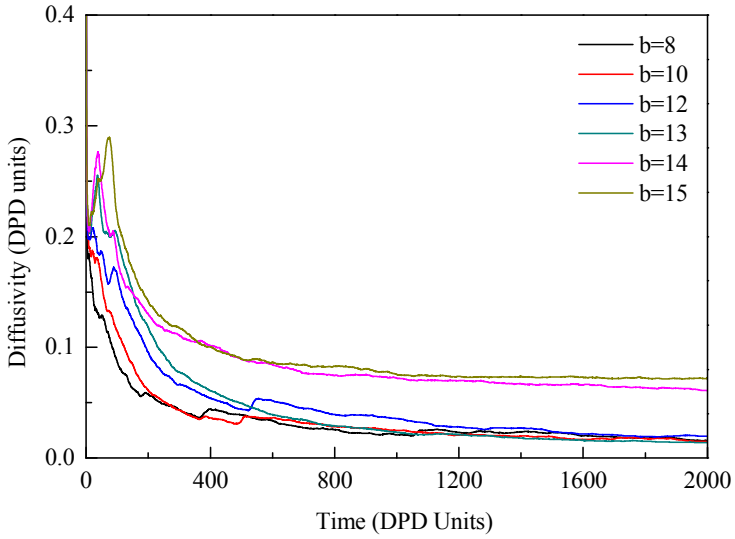

Fig.6 Evolution of the diffusivity of bead ‘b’ with different n-docosane content

Table 1 The molar volumes and solubility parameters of beads

Bead	V_{bead} (cm^3 mol^{-1})	δ (J cm^{-3})
a	18.70	46.51
b	205.93	16.09
c	182.23	15.69
d	108.88	22.625
e	214.68	16.45
f	433.11	22.629
g	112.27	19.76
h	106.05	20.72
i	235.86	16.89
j	583.69	23.37

Table 2 The interaction parameters of beads in PCM system

a_{ij}	a	b	c	d	e	f	g	h	i	j
a	25									
b	162.18	25								
c	150.93	25.03	25							
d	73.04	33.86	34.22	25						
e	164.17	25.03	25.16	33.14	25					
f	195.01	43.05	44.55	25.00	41.32	25				
g	86.84	27.81	28.20	26.21	27.35	27.98	25			
h	79.74	29.41	29.81	25.52	28.86	26.31	25.13	25		
i	172.38	25.20	25.39	32.46	25.07	39.55	26.90	28.30	25	
j	237.84	52.60	54.82	25.26	50.21	25.36	30.98	28.20	47.69	25